

Bulk Aluminum at High Pressures: A First-Principles Study

Michael J. Tambe, Nicola Bonini, and Nicola Marzari*

*Department of Materials Science and Engineering,
Massachusetts Institute of Technology, Cambridge MA 02139*

The behavior of metals at high pressure is of great importance to the fields of shock physics, geophysics, astrophysics, and nuclear materials. We study here bulk crystalline aluminum from first-principles at pressures up to 2500 GPa - soon within reach of laser-based experimental facilities. Our simulations use density-functional theory and density-functional perturbation theory in the local-density and generalized-gradient approximations. Notably, the two different exchange-correlation functionals predict very similar results for the $fcc \rightarrow hcp$, $fcc \rightarrow bcc$, and $hcp \rightarrow bcc$ transition pressures, around 175 GPa, 275 GPa, and 380 GPa respectively. In addition, our results indicate that core overlaps become noticeable only beyond pressures of 1200 GPa. From the phonon dispersions of the fcc phase at increasing pressure, we predict a softening of the lowest transverse acoustic vibrational mode along the [110] direction, which corresponds to a Born instability of the fcc phase around 725 GPa.

First-principles calculations have proved useful to the fields of geophysics,¹ astrophysics,² and nuclear materials.³ Aluminum, being cubic close-packed and having no d -shell electrons, is a prototype for theoretical predictions and understanding the high-pressure behavior of simple metals.⁴ Currently the National Ignition Facility⁵ at LLNL is expected to achieve shockless compression⁶ of metals up to 2000 GPa. This new facility may provide rapid advancements to high-pressure physics and could partner very successfully with theoretical studies.

The equation of state (EOS) and phase stability of aluminum were first studied from first-principles in the early 1980s.^{7,8,9} In all cases the predicted phase sequence was $fcc \rightarrow hcp \rightarrow bcc$, but predictions differed greatly in the transition pressures. Several other calculations within the local-density approximation (LDA)¹⁰ or the generalized-gradient approximation (GGA)^{11,12} have since then been performed, with a predicted static (i.e. without the phonon contribution) $fcc \rightarrow hcp$ transition pressure of 205 ± 20 GPa¹⁰ in LDA and 170 GPa¹¹ and 192 GPa¹² in GGA. These discrepancies are more notable for the $hcp \rightarrow bcc$ transition pressure: 565 ± 60 GPa¹⁰ in LDA versus 360 GPa¹¹ in GGA, leaving significant uncertainties open. Theoretical work on the vibrational properties of aluminum also suggests for the $fcc \rightarrow hcp$ transition a transition pressure higher than the static one.^{11,12} Elastic properties^{13,14} and the absolute strength under tension¹⁵ have also been calculated; the latter results are of particular interest as they demonstrate the important role vibrational modes play in determining mechanical stability and suggest that shear failure modes are inherent in aluminum.

Experimentally, the equation of state of aluminum at high pressures was studied by shock-compression¹⁶ at pressures above the predicted maximum for the $fcc \rightarrow hcp$ phase boundary,¹⁰ but a transition was not observed. However recent diamond anvil cell experiments observed a $fcc \rightarrow hcp$ transition at 217 ± 10 GPa¹⁷ highlighting the difficulty in achieving thermodynamic equilibrium in shock-compression.

In this article we report first-principles calculations

of aluminum under hydrostatic compression up to 2500 GPa. In order to assess mechanical stability under shock, we also calculate the vibrational properties in the fcc phase and determine the elastic constants from the slopes of the phonon dispersions (i.e. the sound velocities).

The equations of state in the fcc , bcc , and hcp phases have been calculated with density-functional theory (DFT) within both LDA¹⁸ and GGA.¹⁹ Calculations have used the QUANTUM-ESPRESSO package.²⁰ We use plane-wave basis sets and pseudopotentials and both 3 electron (3e) norm-conserving pseudopotentials,²¹ with the 3s and 3p electrons in the valence and nonlinear core-corrections, and 11 electron (11e) ultrasoft pseudopotentials²² where the 2s and 2p electrons, usually frozen in the core, are included explicitly in the valence. The inclusion of the 2s and 2p electrons in the valence is essential to investigate the relevance of inner core electrons at high pressure. The planewave cutoffs for the wavefunctions are 25 Ry and 100 Ry for the 3e and 11e pseudopotentials, respectively, and 150 Ry and 800 Ry for the charge density. Brillouin zone integrations have been performed using a cold smearing¹⁴ of 0.02 Ry over shifted Monkhorst-Pack meshes of order $16 \times 16 \times 16$ for the fcc , $22 \times 22 \times 22$ for the bcc and $16 \times 16 \times 10$ for the hcp phases. The large sizes of the k -point meshes are necessary to obtain fully-converged transition pressures. The data for the total energy as function of volume have been fitted to the Birch 3rd order EOS²³ near equilibrium to obtain equilibrium volumes and bulk moduli. The data for the equation of state have been determined from calculations performed at around 50 – 100 different volumes over a pressure range of 0 – 2500 GPa. Finally, the vibrational properties have been computed using density-functional perturbation theory (DFPT).²⁴ The dynamical matrices have been calculated on a $4 \times 4 \times 4$ q -point mesh and Fourier interpolation has been used to evaluate the phonon frequencies on finer grids.

The role of the inner core electrons is of primary concern at very high pressures. Under normal conditions, there is not sufficient overlap between the core and valence shell electrons to question the frozen-core approxi-

TABLE I: The equilibrium lattice parameters, bulk moduli, and transition pressures of Al calculated with the different pseudopotentials described in the text, and compared to experimental results.

	a_0 [Å]	B_0 [GPa]	$fcc \rightarrow hcp$	$fcc \rightarrow bcc$	$hcp \rightarrow bcc$
11e GGA	4.044	73.2	175 GPa	275 GPa	383 GPa
11e LDA	3.985	83.7	172 GPa	272 GPa	380 GPa
3e GGA	4.055	71.8	180 GPa	285 GPa	420 GPa
Expt.	4.025 ^a	78.3 ^a	217 GPa ^b	—	—

^a Ref. 26

^b Ref. 17

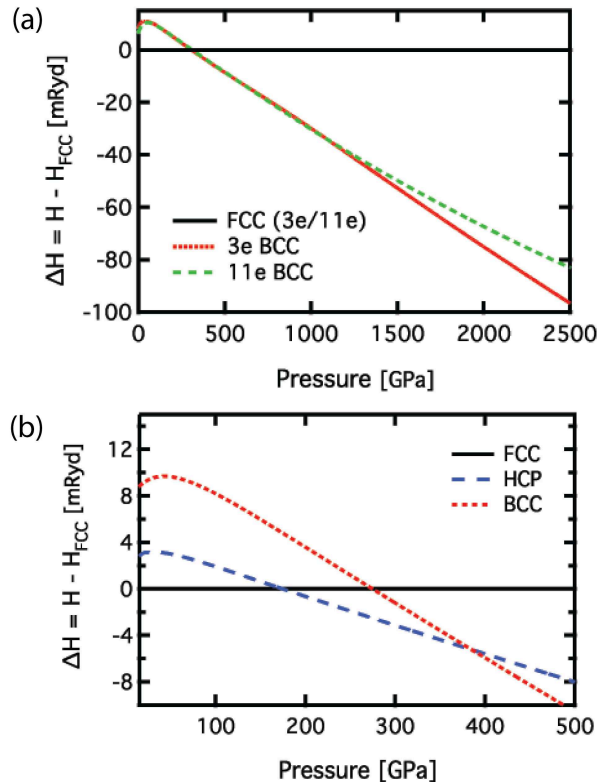


FIG. 1: (a) Enthalpy of the bcc phase (3e and 11e GGA) relative to the enthalpy of the fcc phase (3e and 11e GGA, respectively). (b) Enthalpies for hcp and bcc phase relative to the enthalpy of the fcc phase. The $fcc \rightarrow hcp$, $fcc \rightarrow bcc$, and $hcp \rightarrow bcc$ transition pressures are 175 GPa, 275 GPa, and 380 GPa respectively.

mation,²⁵ but at the pressures considered here core overlaps may become significant. To study the validity of the frozen-core approximation, we first compared the equations of state for different phases using both the 3e and 11e pseudopotentials. We report in Table I the equilibrium lattice parameters and bulk moduli in the fcc phase at zero pressure, and in Fig. 1a the relative enthalpies of fcc and bcc Al with respect to the fcc phase, up to

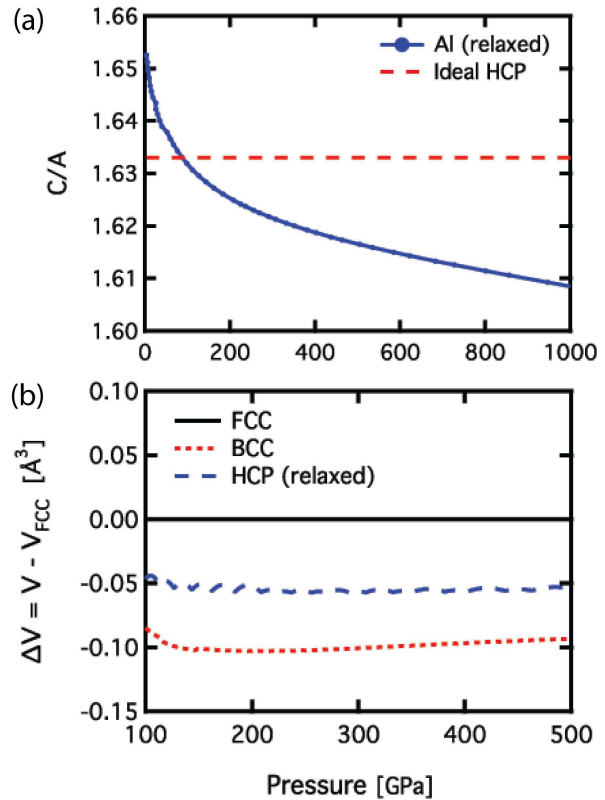


FIG. 2: (a) The c/a ratio of the hcp phase plotted with increasing pressure. (b) Volume versus pressure for the fcc, hcp, and bcc phases plotted relative to the fcc phase.

2500 GPa. These results show that 1) there is little difference between the LDA and GGA predictions, hinting at a broad applicability of density-functional theory in either approximation, and 2) that the role of the core electrons starts to become noticeable only around 1200 GPa, even if already at zero pressure the cores of the 3e pseudopotential start to overlap.²⁷ The equations of state for aluminum in the fcc, bcc and hcp phase, using the 11e GGA pseudopotentials, are shown in Fig. 1b. Although the 11e and 3e calculations give consistent results up to 1200 GPa, the calculated transition pressures can vary, particularly for the $hcp \rightarrow bcc$ transition. This could easily derive from the fact that enthalpy differences between these three phases are only a few mRy (see Fig. 1b), and so, even at full computational convergence of all parameters, small effects (e.g. core-state relaxations), which could shift the calculated enthalpy by less than a mRy, can significantly affect the calculated transition pressures. On the other hand, core electrons seem to have a negligible effect in determining the equilibrium volume, bulk modulus, and even phonon dispersions (see below).

Our LDA and GGA results are consistent with previously reported GGA calculations;^{11,12} discrepancies arise with the LDA results reported in Ref. 10, that predict

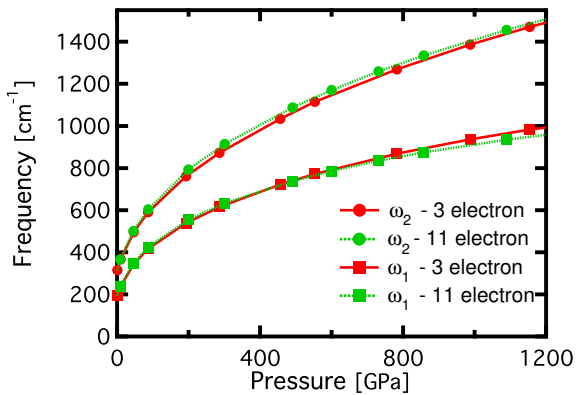


FIG. 3: The frequencies of the two non-degenerate acoustic phonon modes at X calculated with both the 3e and 11e pseudopotentials and plotted as a function of increasing pressure.

205 ± 20 GPa and 565 ± 60 GPa for *fcc* → *hcp* and *hcp* → *bcc* transition pressures, respectively. This discrepancy could arise from Ref. 10 using only 10 – 15 points to fit the equation of state: as reported there, this approximation could significantly affect transition pressures due to the aforementioned small enthalpy differences between competing structures. We also observe that all parameters of the calculation, and particularly the k-point sampling of the Brillouin zone, need to be carefully converged.

Although the pressure that we obtain for the *fcc* → *hcp* transition, 175 GPa, is consistent with previous works^{11,12}, this result is lower than the experimental value of 217 GPa. As suggested in Refs. 11 and 12 this discrepancy could arise from excluding the phonon contribution to the free energy - a hypothesis that should be thoroughly tested, but that is beyond the scope of this brief report.

It should be noted that in our simulations the *hcp* phase was always fully relaxed to identify the optimal, equilibrium *c/a* ratio; this is shown in Fig. 2a. Comparison with experiment at 292 GPa finds agreement in the *c/a* ratio to within 0.1% and well within experimental uncertainty.¹⁷ At 222 GPa the predicted value of the *c/a* ratio differs from experiment by 1%. Since experiments observe a region between 217 and 260 GPa in which the *fcc* and *hcp* phases coexist, this discrepancy is made more reasonable considering that the system might be out of equilibrium. We also show in Fig. 2b the equilibrium volumes for the different phases as a function of pressure. Volume differences between the phases are -0.055, -0.104, and -0.040 Å³ for the *fcc* → *hcp*, *fcc* → *bcc*, and *hcp* → *bcc* transitions respectively, corresponding to volume changes of 0.6(6)%, 1.4(0)%, and 0.6(1)%. We note that in our phase sequence, and in those discussed in the literature,^{7,8,9} only the *fcc*, *hcp*, and *bcc* phases are considered. As a brief self-check we performed variable-cell relaxations at 1000 GPa using a four-atom unit-cell and

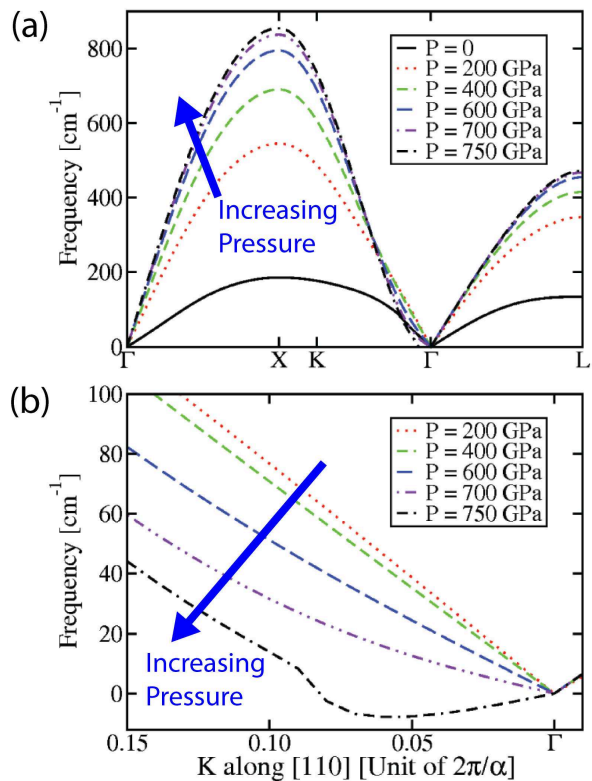


FIG. 4: (a) The lowest energy branch of phonon dispersion for *fcc* Al with increasing pressure. (b) As above, enlarged around Γ , in the $K \rightarrow \Gamma$ direction. A steady flattening is observed with increasing pressure.

five random distinct perturbations. The *bcc* structure was always found.

In order to estimate the dynamical response of aluminum under compression we calculated both the phonon dispersions of the *fcc* phase and the cubic elastic constants (these were derived from the sound velocities, i.e. the slope of the phonons dispersions around Γ) as a function of pressure. Experiments have shown that the *fcc* phase may exist at pressures above the transition pressure either as a super-pressurized phase¹⁶ or as a two phase region.¹⁷ Therefore the mechanical properties of *fcc* aluminum at pressures beyond the equilibrium transition pressure, and any mechanical instabilities that may lead to mechanical failure are relevant to high pressure experiments.

We calculated the phonon dispersions up to 1150 GPa using DFPT. For aluminum this method has been shown to accurately reproduce experimental values at $P=0$.²⁴ Our calculations were performed with the 3e GGA pseudopotential, but compared at selected points in the Brillouin zone with 11e GGA calculations at pressures up to 1200 GPa. As shown in figure 3 the discrepancies between the 3e and 11e results are at most of the order of 3-4% at the highest pressure, and much smaller be-

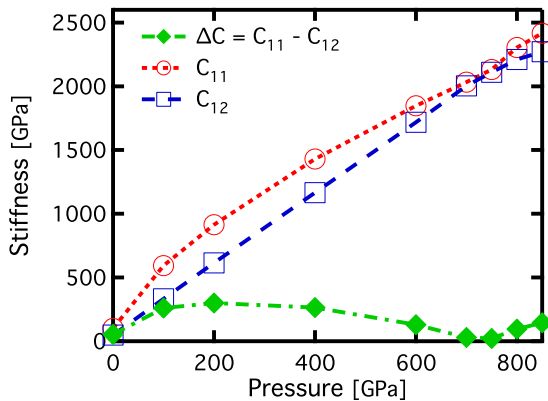


FIG. 5: Elastic constants as obtained from the sound velocities along the [100], [110], and [111] directions. According to the Born criterion the fcc phase becomes mechanically unstable when $\Delta c = c_{11} - c_{12} = 0$; this occurs around 725 GPa.

low that. The phonon dispersions are shown in Fig. 4a and we highlight the appearance, with increasing pressure, of a distinct softening of the lowest energy mode in the [110] direction. This starts to become evident at approximately 400 GPa, and is complete at 725 GPa, as highlighted in Fig. 4b. Since the slope of the dispersion

curves is directly related to the elastic constants (Eq. 1), we can extract the stiffness tensor from the vibrational modes near Γ ; in our case the Born²⁸ criterion for stability is

$$\frac{1}{2}m \left(\frac{1}{\hbar} \frac{\partial E}{\partial k_{110}} \right)^2 = c_{11} - c_{12} \geq 0. \quad (1)$$

As Fig. 5 shows, the stiffness against shear deformation, $\Delta c = c_{11} - c_{12}$, decreases above 400 GPa and goes to zero around 725 GPa, resulting in a Born²⁸ instability. These results complement existing studies of the properties of bulk aluminum^{11,13} and suggest another shear failure mode, supporting previous studies suggesting shear failure modes to be inherent to bulk aluminum.^{13,15} More advanced treatments of mechanical stability including such effects of anharmonic modes²⁴ and internal shear stresses created by loading^{29,30,31} need to be considered in relation to the specific experimental setup before reliable maximum stable pressures can be definitively determined.

Funding for this project has been provided by the U.S. Department of Energy Contract No. DE-FG02-05ER46253. The authors would like to thank A. Dal Corso, I. Dabo, Y.-S. Lee, B. Wood, and J. Garg for useful discussions.

* Electronic address: marzari@mit.edu

- ¹ O.L. Anderson, D. Isaak, and H. Oda, *Rev. Geophys.* **30**, 57 (1992).
- ² A. Alavi, M. Parrinello, and D. Frenkel, *Science* **269**, 1252 (1995).
- ³ J.R. Cheeseman, G.W. Trucks, T.A. Keith, and M.J. Frisch, *J. Chem. Phys.* **104**, 5497 (1996).
- ⁴ R.M. Martin, *Nature* **400**, 117 (1999).
- ⁵ A. Heller, *Science and Technology Review* 4 July/August (1999); <https://lasers.llnl.gov/>
- ⁶ J. Edwards, K.T. Lorenz, B.A. Remington, S. Pollaine, J. Colvin, D. Braun, B.F. Lasinski, D. Reisman, J.M. McNaney, J.A. Greenough, R. Wallace, H. Louis, D. Kalantar, *Phys. Rev. Lett.* **92**, 075002 (2004).
- ⁷ J.C. Boettger and S.B. Trickey, *Phys. Rev. B* **29**, 6434 (1984).
- ⁸ P.K. Lam and M.L. Cohen, *Phys. Rev. B* **27**, 5986 (1983).
- ⁹ A.K. McMahan and J.A. Moriarty, *Phys. Rev. B* **27**, 3235 (1983).
- ¹⁰ J.C. Boettger and S.B. Trickey, *Phys. Rev. B* **53**, 3007 (1996).
- ¹¹ G.V. Sin'ko and N.A. Smirnov, *J. Phys.: Cond. Matt.* **14**, 6989 (2002).
- ¹² F. Jona and P.M. Marcus, *J. Phys.: Cond. Matt.* **18**, 10881 (2006).
- ¹³ W. Li and T. Wang, *J. Phys.: Cond. Matt.* **10**, 9889 (1998).
- ¹⁴ N. Marzari, D. Vanderbilt, A. DeVita, and M.C. Payne, *Phys. Rev. Lett.* **82**, 3296 (1999).
- ¹⁵ D.M. Clatterbuck, C.R. Krenn, M.L. Cohen, and

- J.W. Morris, *Phys. Rev. Lett.* **91**, 135501 (2003).
- ¹⁶ W.J. Nellis, J.A. Moriarty, A.C. Mitchell, M. Ross, R.G. Dandrea, N.W. Ashcroft, N.C. Holmes, and G.R. Gathers, *Phys. Rev. Lett.* **60**, 1414 (1988).
- ¹⁷ Y. Akahama, M. Nishimura, K. Kinoshita, H. Kawamura, and Y. Ohishi, *Phys. Rev. Lett.* **96**, 045505 (2006).
- ¹⁸ J.P. Perdew and A. Zunger, *Phys. Rev. B* **23**, 5048 (1981).
- ¹⁹ J. P. Perdew, K. Burke, and M. Ernzerhof, *Phys. Rev. Lett.* **77**, 3865 (1996).
- ²⁰ P. Giannozzi *et al.*, <http://www.quantum-espresso.org>.
- ²¹ A. M. Rappe, K.M. Rabe, E. Kaxiras, and J. D. Joannopoulos, *Phys. Rev. B* **41**, 1227 (1990).
- ²² D. Vanderbilt, *Phys. Rev. B.* **41**, 7892 (1990).
- ²³ F. Birch, *Phys. Rev.* **71**, 809 (1947).
- ²⁴ S. Baroni, S. de Gironcoli, A. Dal Corso, and P. Giannozzi, *Rev. Mod. Phys.* **73**, 515 (2001).
- ²⁵ T.L. Gilbert, *Phys. Rev. B* **12**, 2111 (1975).
- ²⁶ R. Stedman and G. Nilsson, *Phys. Rev.* **145**, 492 (1966).
- ²⁷ The core radius of the 3e pseudopotential is 1.43 Å; the half-bond length at 0 GPa is also 1.43 Å, decreasing to 0.93 Å at 1200 GPa. RRKJ²¹ pseudowavefunctions closely reproduce all-electron wavefunctions even for radii smaller than the matching radius, partially explaining the good results obtained with the 3e pseudopotential.
- ²⁸ M. Born, *Proc. Cambridge Philos. Soc.* **36**, 160 (1940).
- ²⁹ R. Hill and F. Milstein, *Phys. Rev. B* **15**, 3087 (1977).
- ³⁰ J. Wang, J. Li, S. Yip, S. Phillpot, and D. Wolf, *Phys. Rev. B* **52**, 12627 (1995).
- ³¹ F. Milstein, *Handbook of Material Modeling*, 1223

(Springer, 2005).